Chapter 3

Coiled-coil Peptide Dimers Enhance Liposomal Drug Delivery

Abstract

An ideal nanomedicine design improves the therapeutic efficacy of a drug. However, most nanomedicines enter the cell via endosomal/lysosomal pathways and typically only a small fraction of cargo enters the cytosol inducing a therapeutic effect. To circumvent these inefficient drug delivery pathways, alternative approaches are desired. SNARE proteins, and related peptide mimics, mediate the fusion of membranes and can be used to trigger fast, productive drug delivery *in vitro* and *in vivo*. Previously we used the heterodimeric peptide pair E/K to induce membrane fusion. In this study, we synthesized dimeric coiled-coil peptide variants of peptide K to facilitate liposome fusion with peptide E modified liposomes and cells. Various dimer designs were compared and the parallel PK4 dimer induced the strongest coiled-coil interaction resulting in a higher cellular uptake of the liposome-encapsulated cargo, as compared to linear dimer designs. Using a wide spectrum of endocytosis inhibitors, it was shown that membrane fusion was the main cellular uptake pathway. Delivery of the antitumor drug doxorubicin (DOX) resulted in enhanced cellular delivery and concomitant antitumor efficacy *in vitro*. These findings not only offer important mechanistic insights into the design of coiled-coil driven membrane fusion systems but also provide novel strategies to develop peptide-based biomaterials.

Introduction

During the last decades, nanomedicines with improved drug delivery efficiency have been developed by amplifying drug bioavailability, improving pharmacokinetic/pharmacodynamic profiles, and/or minimizing undesired off-target or other side effects of encapsulated drugs.[1-3] Several nanomedicines based on liposomes, albumin NPs, and polymeric micelles have been approved for cancer treatment and several nanomedicine candidates for chemotherapy, hyperthermia, radiation therapy, gene therapy, and immunotherapy are in clinical trials.[4-6] Nanomedicines have been customized to enter cells through different endocytosis pathways, delivering their cargo to the cell.[7, 8] However, endocytosis often impedes drug delivery efficiency since the majority of the nanomedicine cargo faces endo/lysosome degradation, lowering the therapeutic efficacy. Therefore, novel drug delivery systems circumventing endo/lysosome pathways and/or entrapment would greatly enhance intracellular drug delivery efficiency.

Peptides have attracted great attention in the nanomedicine field due to their diversity and ease of modification and conjugation to drug delivery nanoparticles.[9, 10] For example, cell-penetrating peptides (CPP) have been widely investigated for their cell-penetrating abilities[11, 12] and chemically synthesized CPPs covalently or noncovalently conjugated to biomaterials greatly enhanced cell penetration and drug efficacy.[13, 14] Besides direct penetration, CPP-cargo conjugates mainly gain their entry to the cells through energy-dependent endocytosis, such as macropinocytosis or clathrin-mediated endocytosis.[15-17] Moreover, CPP dimerization significantly lowered the cell-penetrating concentration required by efficient Tat–TAR interaction inhibition of HIV-1,[11] and achieved potent antitumor effects.[18, 19] Based on the advances made in this field, various CPP-derived peptide therapeutics have been clinically evaluated.[20-23] Unfortunately, to date there are no CPP-based drug conjugates/nanomedicines approved by the FDA. This might be due to their lack of cell and tissue specificity, drug delivery inefficiency, slow drug release profile, poor stability, rapid renal clearance, and severe adverse effects like high toxicity.[21, 24, 25]

Thus there is still a pressing need to find alternatives to deliver drugs efficiently into cells. Membrane fusion is a vital process for the transport of (bio)chemicals across membranes in eukaryotic cells, from the exquisite compartmental organization of cells to the precise timing of chemical synaptic transmission of nervous system activities.[26-28] The docking of transport vesicles to the target plasma membrane in neuronal exocytosis is triggered by the coiled-coil formation of complementary SNARE protein subunits.[27] Inspired by the SNARE protein complex to trigger the membrane fusion process between liposomes and cells, we previously developed complementary pairs of coiled-coil peptides K/E conjugated to lipids able to trigger membrane fusion, inducing fast and efficient liposomal drug delivery *in vitro* and *in vivo*.[29-31] Peptide K is an amphipathic helical peptide and was specifically designed to interact with peptide E, but when confined to a membrane, it also interacts with lipid bilayers.[32]

Due to this dual affinity to both peptide E and lipid membranes, in this chapter, we investigate whether dimerization of peptide K could enhance liposomal drug delivery to cells. The influence of peptide dimerization on their solution properties was studied as well as the ability to induce fusion of liposomes with cells to control drug delivery (**Scheme 1**). By varying the position of peptide conjugation, three novel dimer designs were synthesized. Coiled-coil interactions and cell membrane

binding affinities were compared by circular dichroism spectroscopy and flow cytometry measurements. Next, the cellular uptake of liposomes was also evaluated by flow cytometry and confocal microscopy. The *in vitro* antitumor effect of the chemotherapeutic doxorubicin (DOX) encapsulated in liposomes was quantified as a function of dimer design. This study could aid the development of efficient delivery systems of drugs into cells using liposome-cell fusion.

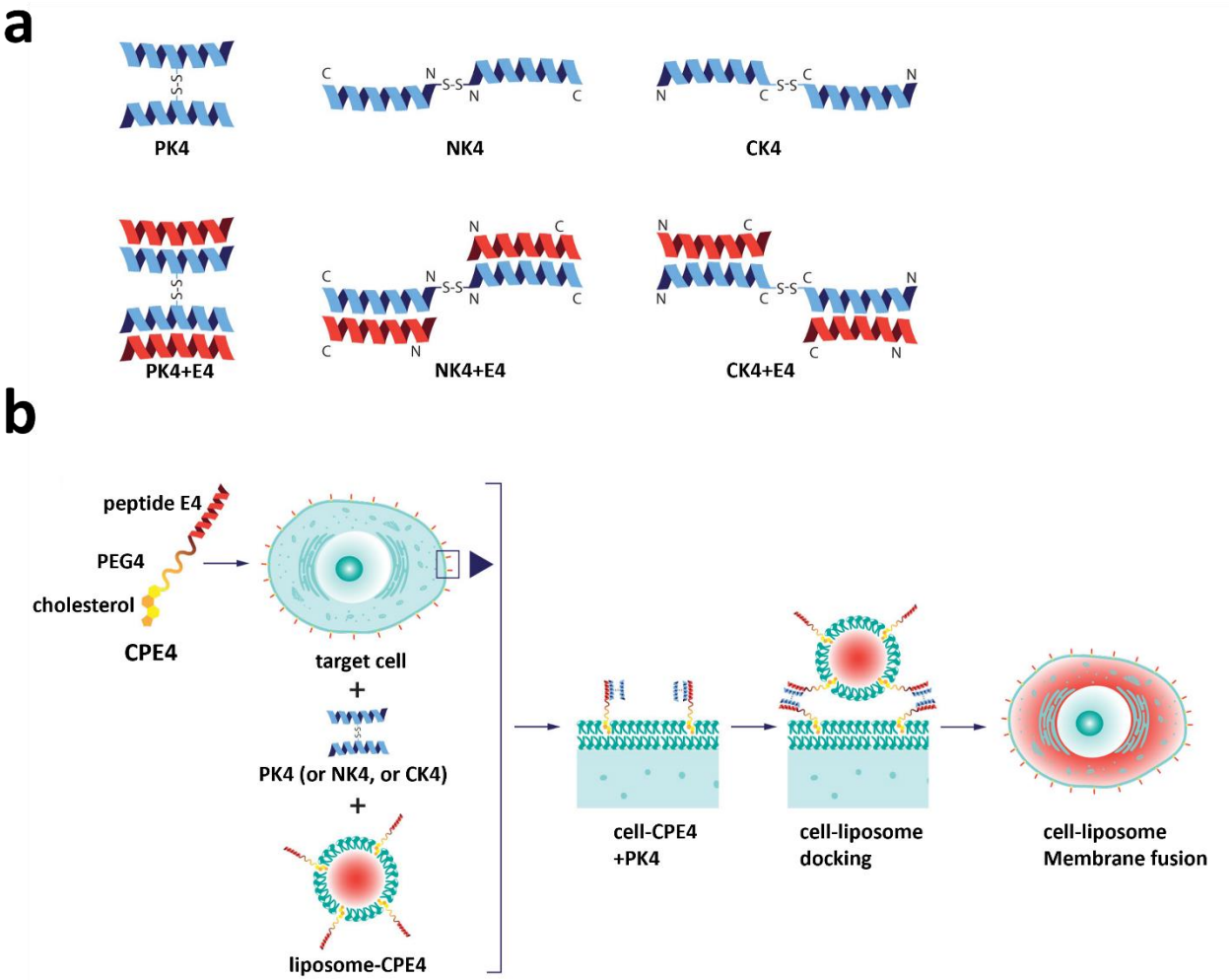

Scheme 1. **Schematic illustration of the cell-liposome membrane fusion process trigged by K4-dimers and E4.** (**a**) schematic representation of K4-dimers and coiled-coil structure of K4-dimers with complementary E4. (**b**) Liposomal drug delivery to cells through membrane fusion induced by different coiled-coils.

Results and discussion

Peptide design

Peptide K was previously designed to form a parallel heterodimeric coiled-coil complex with peptide E,[32] but we discovered it also has a high affinity to fluid phospholipid membranes. Upon binding, peptide K induces positive membrane curvature and destabilization, facilitating membrane fusion.[33-35] Due to these competing interactions, we rationalized that a Peptide K-dimer might interact simultaneously with peptide E as well as with a membrane, resulting in enhanced fusion. How these

dual interactions will result in membrane fusion is most likely dependent on the exact structure of these dimers. In this study, we designed three K4-dimers by peptide K4 dimerization via a disulfide bond. For this, a cysteine was introduced at either the N- or C-terminus, or at the f-position in the 2nd heptad of peptide K. Upon oxidative dimerization the parallel dimer PK4 and the linear dimers NK4 (N-terminal conjugation) and CK4 (C-terminal conjugation) were obtained (**Scheme 1a**). Based on the structure, linear K4-dimers may form a 'tetramer-like' homodimer structure or a hairpin structure, stabilizing the α-helix structure. Since the hydrophobic faces of both K peptides are oriented in opposite directions, it was expected that PK4 may not be able to dimerize, but rather interact with other dimers resulting in aggregation.

The secondary structure of the peptide dimers and their ability to interact with peptide E was studied using circular dichroism (CD) spectroscopy. In line with previous studies, peptide K4 folds into an α-helix as evidenced by the two minima at 208 and 222 nm. Peptides NK4 and CK4 also adopt a highly helical conformation comparable to monomeric K4. In contrast, PK4 adopted a skewed non-α-helix spectrum, indicative of aggregation (**Fig. 1a, Table S3**). Peptide E4 adopts an α-helical secondary structure and upon mixing with equimolar PK4 coiled-coil formation was observed (**Fig. 1b**). The helicity observed for the PK4+E4 mixture is much higher as compared to the calculated average, which assumes no interaction (**Table S3**). The linear dimer NK4 also adopts an α-helical structure, and the helicity increased upon mixing with E4 (**Fig. 1c, Table S3**). In contrast, the CD-spectrum of a mixture of linear dimer CK4 and E4 did not indicate effective coiled-coil formation (**Fig. 1d, Table S3**). This suggests that the 'tetramer-like' homodimer or helical hairpin of CK4 is too stable, preventing interaction with E4, but the less stable homodimer of NK4 does form heteromeric coiled coils with E4, and the parallel PK4 forms highly enhanced coiled-coil interactions with E4.

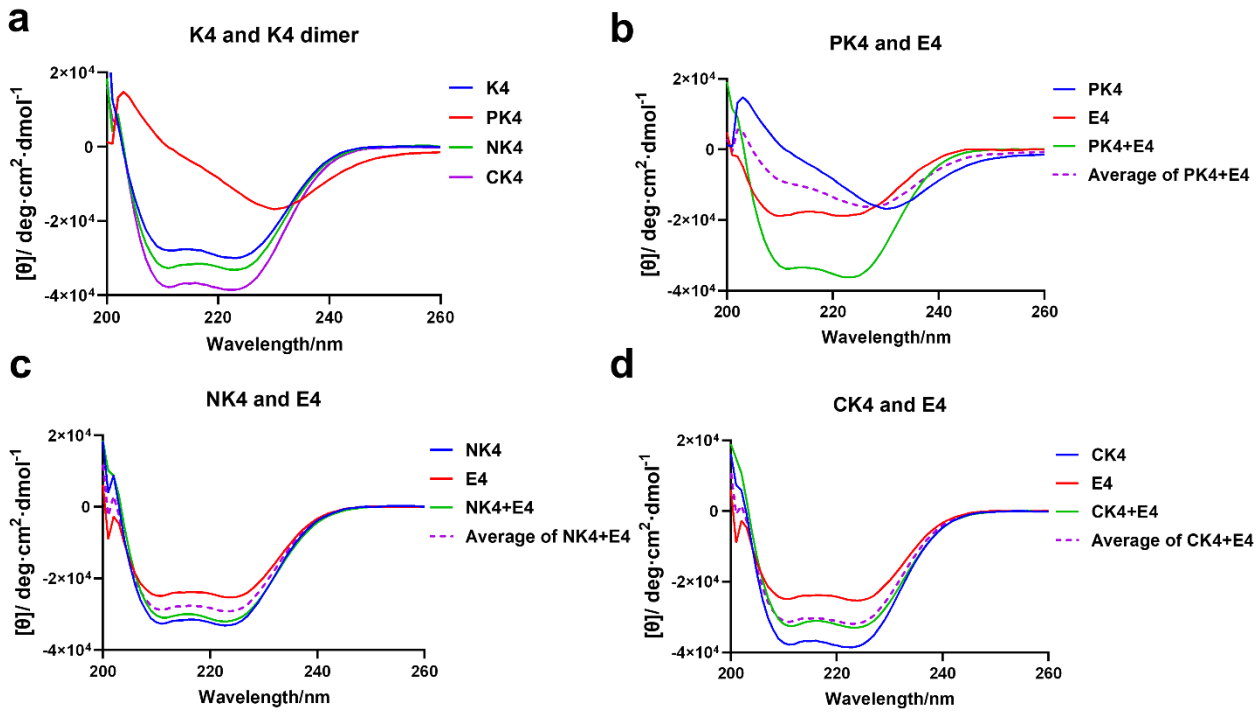

Figure 1. CD spectra of (**a**) K4 monomer and K4-dimers, (**b**) PK4 ± E4, (**c**) NK4 ± E4, and (**d**) CK4 ± E4. Solid

lines are measured spectra, dotted lines are calculated average spectra from the K4-dimers and peptide E4. Spectra were recorded in PBS (pH 7.2) at 20 °C. K4-dimer, 5 μM; K4 monomer, 10 μM; E4, 10 μM.

Cell membrane labeling efficiency between dimers

In previous studies, the addition of a fluorescently labeled E4 peptide, dubbed Fluo-E4, to CPK4-pretreated cells resulted in a uniformly fluorescent cell membrane due to the formation of coiled coils between CPK4 and Fluo-E4. To confirm whether coiled-coil formation between K4-dimers and E4 also occurs at the surface of cells, a cell membrane labeling assay was performed. HeLa cells were preincubated with CPE4 as described previously.[31] Next, the cells were treated with the various K4-dimers and finally carboxyfluorescein-labeled E4 (Fluo-E4) was added (**Fig. 2a**). Interestingly, cell membrane labeling efficiency varied between the various K4-dimers (**Fig. 2b**). PK4 displayed the highest fluorescence on the cell membrane, indicating efficient coiled-coil formation between PK4 and CPE4. In contrast, the linear K4-dimers NK4 and CK4 showed a lower degree of fluorescence. We also studied the importance of pretreating cells with CPE4. Plain cells incubated with PK4 also exhibited membrane binding albeit the observed fluorescence was not homogeneously distributed (**SI Fig. 1a**). Most likely, the positively charged PK4 peptides form aggregates in solution which bind to the negatively charged cell membrane via attractive electrostatic interactions. The addition of the linear dimers NK4 or CK4 to plain cells did not result in any detectable binding.

The differences in binding of the various K4-dimers was quantified by flow cytometry (**Fig. 2c**). CPE4 pretreated cells revealed a high binding affinity for K4 and K4-dimers. In contrast, in the absence of CPE4 hardly any peptide K(-dimer) binding was observed. These results were consistent with the CD and confocal imaging results. PK4-dimer associated effectively with the cell membrane by either forming coiled-coils with CPE4 or directly interacting with the cell membrane. In contrast, the linear dimers NK4 and CK4 showed a weaker ability to induce coiled-coil interactions, resulting in a low cell membrane affinity.

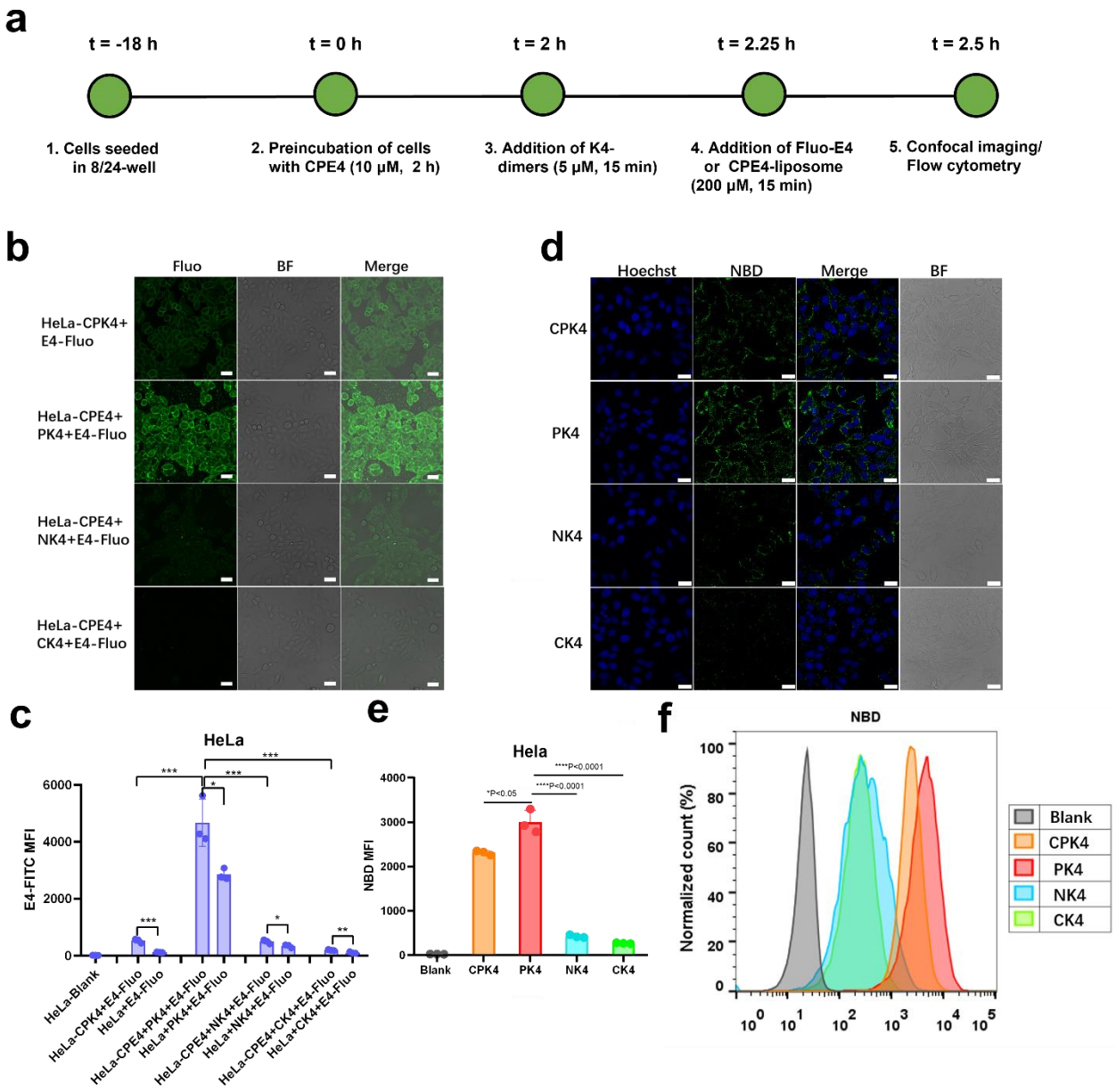

Figure 2. Cell labeling and cell uptake studies. **(a)** Schematic representation of the cell labeling and cell uptake experiments of K4 dimer with cells. (**b**) Confocal images of cell membrane labeling between K4 monomer and dimers with complementary Fluo-E4. Green: fluorescein-E4; BF: bright field; scale bar is 30 μm. **(c)** Quantification of cell membrane labeling efficiency by flow cytometry measurements. **(d)** Confocal images of K4 monomer and dimers with fluorescent NBD-PE labeled CPE4-liposomes. **(e-f)** Quantification of NBD-liposome intensity between monomer and dimers. Green: NBD-PE; blue: Hoechst 33342. BF: bright field; scale bar is 30 μm. Unpaired student t-test was used to determine the significance of data comparisons (****$P < 0.0001$; ***$P < 0.001$; **$P < 0.01$; *$P < 0.05$). In all panels, error bars represent mean ± s.d. (n=3).

Cell uptake efficiency of dimers

After examining coiled-coil formation at the cell membrane between the K4-dimers and CPE4, cell uptake of CPE4-liposomes was investigated using the same approach. Again, cells were preincubated sequentially with CPE4 and the K4-dimers before fluorescent CPE4-liposomes were added and cell

uptake was quantified (**Fig. 2a**). As expected, CPE4-liposomes were homogeneously distributed on the cell membrane (**Fig. 2d**). However, marked differences were observed for the different K4-dimers. PK4 induced strong and enhanced cell-liposome uptake efficiency, while the linear dimers NK4, and CK4 were less efficient. When the CPE4 preincubation step of cells was omitted, PK4 also induced some binding, but the fluorescence was randomly dispersed on the cell membrane (**SI Fig. 1b**). As mentioned earlier, attractive interactions between PK4 and the cell membrane might be the cause for this observation. As expected, the linear dimers NK4 and CK4 were unable to bind to cells without CPE4 preincubation. The cell uptake efficiency differences between groups was again quantified with flow cytometry (**Fig. 2e-f**). Consistent with confocal imaging, the PK4 coiled-coil pair showed the highest cell uptake efficiency, which was superior to monomeric K4 and the linear dimers NK4 and CK4. Not surprisingly, in cells without CPE4 preincubation, the dimers resulted in weaker cell uptake efficiency (**SI Fig. 1c**). Combined, these studies revealed that PK4 interacts very efficiently with CPE4-preincubated cells.

Liposome-cell membrane fusion --NBD/propidium iodide (PI) delivery of dimers

Next, membrane fusion between liposomes and cells was studied using propidium iodide (PI) as a model drug. This dye binds to DNA and is membrane impermeable requiring a drug delivery carrier to enter cells. Cells were sequentially pretreated with CPE4 and the K4-dimers before PI encapsulated in CPE4-liposomes was added to induce liposome-cell membrane fusion and concomitant PI delivery (**Fig. 3a**). Confocal imaging showed the green fluorescent dye NBD incorporated in CPE4-liposomes, evenly distributed on cell membranes, while PI was observed in the cytosol and nucleus of cells (**Fig. 3b**). As expected, CPK4-liposomes are able to deliver PI into cells, consistent with our previous study.[31] Importantly, PK4 induced the highest PI delivery inside cells and the dye was present in the cytosol and nucleus. In contrast, the linear K4-dimers induced only a low PI delivery efficiency. NK4 induced weak fluorescence both on the cell membrane and in the cytoplasm, and almost no membrane and cytoplasm fluorescence was observed when CK4 was used. When the cells were not pretreated with CPE4, PK4 was still able to induce liposome-cell fusion resulting in some PI uptake (**SI Fig. 2a**). Furthermore, liposomes lacking CPE4 showed neither PI delivery nor NBD-labeling of the cell plasma membrane irrespective of the K-dimer used (**SI Fig. 2b**). Next, the same experiment was performed using Chinese hamster ovary (CHO) cells to confirm that PI delivery is cell-type independent. Consistent with the previous studies in HeLa cells, PI was observed in CHO cells when PK4 was used, while CPK and the linear K-dimers were less efficient (**SI Fig. 3a**). Again, omitting the CPE4 preincubation step resulted in inefficient PI delivery (**SI Fig. 3b**).

In summary, these results revealed that all K4-dimers mediate cell-liposome membrane fusion resulting in cytosolic and nuclear PI delivery. The PK4-dimer outperformed all other designs due to the enhanced coiled-coil interaction between PK4 and E4, combined with the membrane affinity of PK4 facilitating efficient PI delivery efficiency.

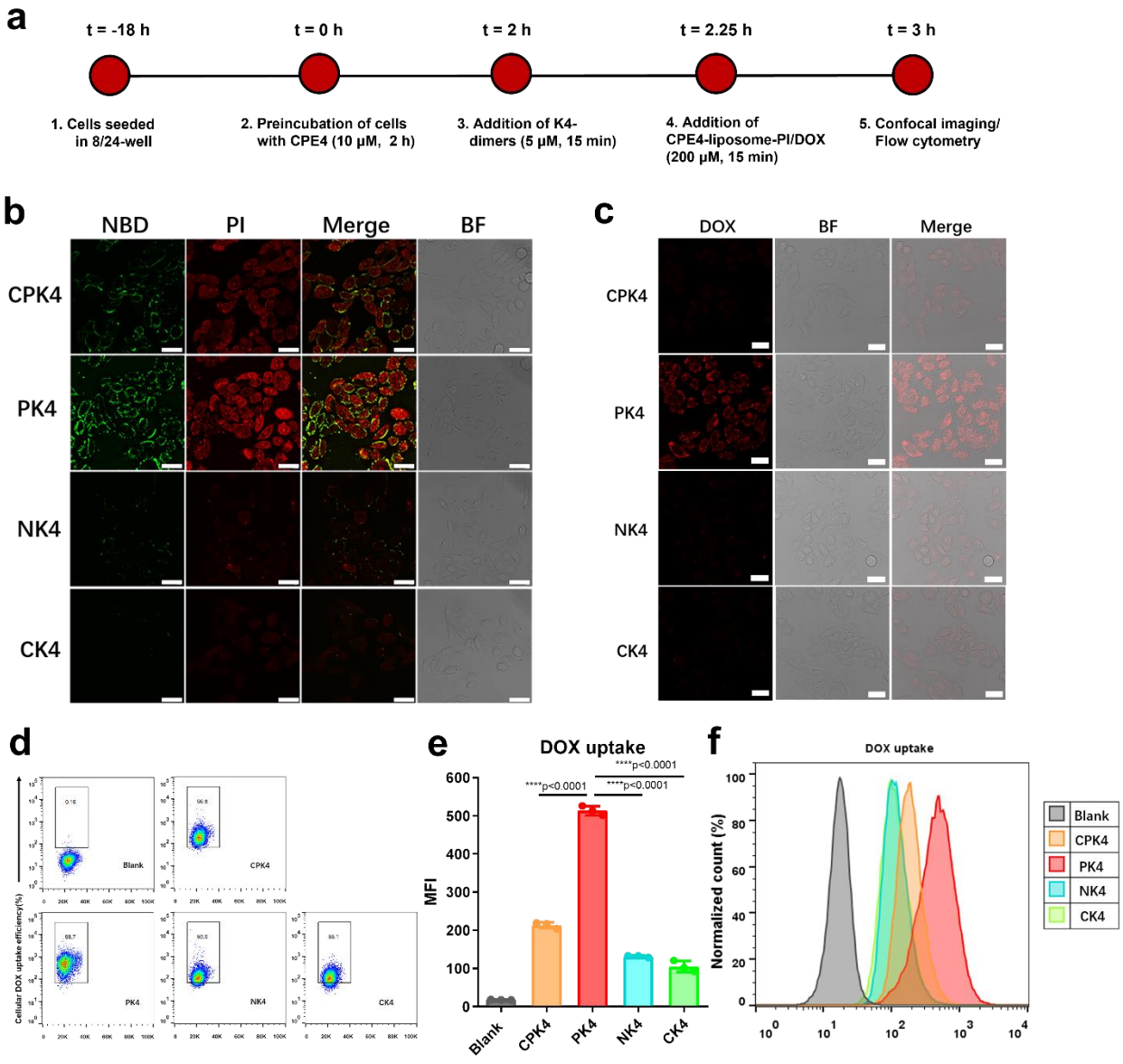

Figure 3. **Liposomal delivery (PI and DOX) to cells. (a)** Schematic representation of the liposomal delivery of PI and DOX to cells. **(b)** Confocal images of liposomal PI delivery by K4 monomer and dimers. Green: NBD-PE; red: PI; BF: bright field; scale bar is 30 μm. **(c)** Confocal images of DOX uptake facilitated by K4 monomer and dimers in HeLa cells. Red: DOX; BF: bright field; scale bar is 30 μm. **(d)** Quantification of DOX uptake percentages facilitated by K4 monomer and dimers in HeLa cells. **(e-f)** Quantification of internalized DOX intensity facilitated by K4 monomer and dimers. Unpaired student t-test was used to determine the significance of data comparisons (****P < 0.0001; ***P < 0.001; **P < 0.01; *P < 0.05). In all panels, error bars represent mean ± s.d. (n=3).

Delivery of doxorubicin.

After proving that K4-dimers efficiently mediate liposomal PI delivery into cells via membrane fusion, drug delivery efficiency and subsequent pharmacological effects were further evaluated using doxorubicin (DOX) (**Fig. 3a**). This drug is an effective and frequently used chemotherapeutic agent for various malignancies, but cardiomyopathy is a life-threatening side effect.[36, 37] Therefore targeted DOX delivery is highly desired because it would increase the therapeutic dose while limiting the side effects. Furthermore, DOX becomes more fluorescent upon binding to DNA and tRNA, making it

suitable for cellular imaging and quantification.

CPE4-preincubated cells were treated with the K4-dimers before CPE4-liposomes containing DOX were added. Confocal imaging confirmed successful DOX delivery as its fluorescence was observed in both the nucleus and cytosol of cells (**Fig. 3c**). Again, PK4 induced the most effective DOX cellular delivery, as compared to the linear K4-dimers or CPK4. Untreated cells showed negligible DOX delivery confirming that CPE4 and K4-dimers are required for efficient drug delivery (**SI Fig. 4a**).

DOX delivery was quantified by flow cytometry. All coiled-coil pairs facilitated liposome-cell fusion resulting in a high percentage of DOX positive cells, >85% in all cases (**Fig. 3d**), indicative of successful DOX delivery. Importantly, the internalized DOX intensities varied significantly between the groups. In line with all previous results, PK4 achieved the highest DOX intensities in cells as compared to CPK4 and the linear K4-dimers (**Fig. 3e-f**). DOX was delivered by PK4 to cells that were not pretreated with CPE4, albeit with a lower intensity than CPE4-preincubated cells. All control groups did not show significant DOX delivery (**SI Fig. 4b**). These results demonstrate that the CPE4/PK4 pair achieved the highest DOX delivery in all experimental groups.

DOX uptake efficiency after endocytosis inhibitors

CPE4/CPK4-mediated fusion of liposomes with cells was confirmed in a previous study using well-known endocytosis inhibitors.[31] In this study, PK4 was the most efficient at delivering content to cells and therefore we studied the uptake mechanism in the presence of common endocytosis inhibitors. After incubation of cells with the endocytosis inhibitors, uptake of liposomes and concomitant delivery of content was quantified. Flow cytometry was employed to quantify the intensity differences of internalized DOX with each endocytosis inhibitor treatment and compared to delivery in the absence of the inhibitors. Since the PK4-dimer is positively charged, we included cationic liposomes (DOTAP: DOPC, 1:1) in this study for comparison.

Nocodazole is an inhibitor of micropinocytosis, a microtubule-disrupting agent that prevents tubule formation and leads to the distribution of IgA-containing vesicles throughout the cytoplasm.[38] Wortmannin blocks PI3-kinase activity and acts as a micropinocytosis inhibitor.[39, 40] Dynasore is reported to inhibit GTPase and dynamin activities reversibly,[41] which is indispensable for clathrin-mediated and caveolae-mediated endocytosis in eukaryotic cells.[42, 43] Pitstop 2 is an inhibitor of clathrin-mediated endocytosis as it blocks the endocytotic ligand association with the clathrin terminal domain.[44, 45] Genistein blocks the tyrosin-phosphorylation process in Cav 1 and caveola-dependent endocytosis.[46, 47] Methyl-β-cyclodextrin (MβCD) is usually used to determine whether the endocytosis is dependent on the integrity of lipid rafts.[47, 48] Sodium azide (NaN_3) is an ATP energy depletion agent that inhibits cytochrome C oxidase in the mitochondria of cells.[49]

The cellular uptake of cationic liposomes was greatly inhibited in the presence of NaN_3, MβCD, wortmannin and incubation at 4 °C. This experiment revealed that cationic liposome uptake is energy-dependent, mainly driven by micropinocytosis and depends on lipid raft integrity (**SI Fig. 5a**).[50]

Next, the effect of endocytosis inhibitors on cellular uptake of liposomes encapsulating DOX using the PK4 coiled-coil dimer was investigated (**Fig. 4a**). Most of the endocytosis inhibitors seemed to have a minimal effect on DOX uptake efficiency except for MβCD, which disrupts the cholesterol-

rich caveolae-containing membrane microdomains by removing cholesterol from the plasma membrane.[51] Unlike the cationic DOTAP liposomes, the ATP energy depletion agent NaN_3 exerted no effect on the uptake efficiency for PK4-dimer, only the 4 ℃ incubation reduced the uptake efficiency slightly. This demonstrated that the cellular uptake of the PK4-dimer was mainly driven by membrane fusion independent of energy consumption, and also demands lipid integrity. We also tested the endocytosis inhibitors' effect on the PK4-dimer when the cells were not pretreated with CPE4 (**SI Fig. 5b**). Similar to the PK4 coiled-coil pair, MβCD and 4 ℃ incubation resulted in major cellular uptake reduction. Meanwhile, nocodazole and dynasore reduced the cellular uptake by about 25% and 15% respectively, indicating micropinocytosis and clathrin-mediated endocytosis were also involved. Taken together, these results prove that cellular DOX uptake of the PK4-dimer was mainly induced by membrane fusion requiring the presence of cholesterol. Due to the positive charges of the PK4 particles, it could also partially facilitate the lipopeptide CPE4-modified liposomes entering the cell through endocytosis, and this could further facilitate cellular delivery.

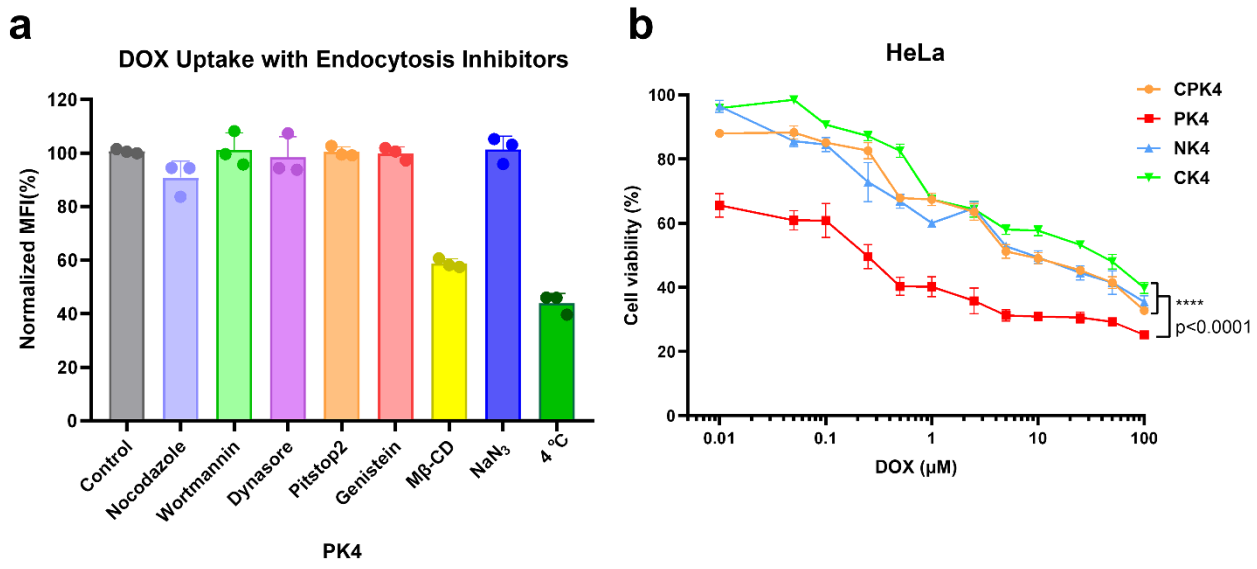

Figure 4. (a) Quantification of DOX uptake efficiency of HeLa cells with endocytosis inhibitors in the presence of the PK4-dimer pair. **(b)** Cytotoxicity evaluation of K4 monomer and dimers after delivery of DOX. Two-way ANOVA analysis was used to determine the significance of data comparisons (****P < 0.0001; ***P < 0.001; **P < 0.01; *P < 0.05). In all panels, error bars represent mean ± s.d. (n=3).

In vitro antitumor effect evaluation after delivery of DOX

After confirming that CPE4/PK4 delivers liposomal DOX efficienctly into cells, the antitumor effect induced by DOX delivery was evaluated. HeLa cells were decorated with CPE4, treated with the K4-dimers and then incubated for 2 h with CPE4-modified liposomes encapsulating DOX. Next, the cell viability was determined after 36 h. Efficient DOX cellular uptake requires both peptides to be present, thus we mainly focused on the comparison of the HeLa cytotoxicity differences between K4 monomer and dimers in which both peptides were included after the delivery of DOX. The K4 monomer and dimers induced an *in vitro* antitumor effect in a concentration-dependent manner (**Fig. 4b**). The parallel PK4-dimer induced potent cytotoxicity, and the viability of HeLa cells was

significantly lower than with the monomer and linear dimers for all the concentrations, demonstrating an improved antitumor effect by PK4-mediated delivery of DOX.

An MTT assay was used to proof that the peptides and lipomes in the absence of DOX were non-toxic. For this, cells were decorated with CPE4 and the K4-dimers were added, followed by the addition of CPE4 modified liposomes (without encapsulated DOX). The cell viability remained above 90% for all liposome concentrations, demonstrating the drug delivery system itself was biocompatible and presented no obvious cytotoxicity (**SI Fig. 5c**). Taken together, we showed that coiled-coil peptide dimers can be safely applied to facilitate cellular drug delivery, and the CPE4/PK4 pair can induce highly efficient cellular liposomal delivery with an enhanced therapeutic effect after loading antitumor drugs into the liposomes.

Conclusion

We designed three coiled-coil peptide-K dimers by varying the conjugation position and investigated their structural differences, cellular uptake efficiency, and pharmacological effects after encapsulating an antitumor drug. CD spectroscopy revealed distinctive differences in helical structures between dimers, where PK4 exhibited the strongest coiled-coil interactions with the complementary peptide E4. The cell membrane labeling assay showed that PK4 triggered the highest cell membrane affinity while linear K4-dimers hardly interacted with the cell membrane. Cellular uptake studies showed liposome delivery into cells was depending on the dimer used. Among the three dimers, PK4 elicited the strongest cellular liposomal delivery and DOX cellular uptake. The uptake mechanism study proved that the efficient liposomal DOX delivery achieved using PK4, was mainly mediated by membrane fusion, although endocytosis was partially involved due to the non-specific interactions between positively charged PK4 and cell membranes. Consistent with the DOX cellular uptake result, a cytotoxicity evaluation confirmed PK4 induced an enhanced antitumor effect *in vitro*, which was superior to CPK4 and the linear dimers NK4 and CK4. These results indicate that PK4 possesses the strongest coiled-coil interaction with peptide E, leading to significant membrane fusion and concomitant efficient cellular liposomal delivery. Moreover, the high affinity of PK4 to lipid membranes aids fusion. In comparison, coiled-coil formation of linear dimers is notably weak and their lipid membrane affinity is also low, therefore they are unable to induce efficient membrane fusion. These results confirm our hypothesis that dimerization of peptide K could increase membrane fusion and lipid affinity, which is pivotal for achieving enhanced liposomal drug delivery. In summary, this study of peptide dimerization design and their cellular delivery evaluation not only contributes to the design and development of coiled-coil peptide-based membrane fusion systems but also provides a more efficient system for future drug delivery applications.

Methods

Chemicals and reagents

All Fmoc-protected amino acids were purchased from Novabiochem. Piperidine, trifluoroacetic acid, acetonitrile, dimethylformamide (DMF), dichloromethane (DCM), and ethanol were purchased from Sigma-Aldrich. 1,2-dioleoyl-*sn*-glycero-3-phosphocholine (DOPC), 1,2-dioleoyl-*sn*-glycero-3-phosphoethanolamine (DOPE), 1,2-dioleoyl-*sn*-glycero-3-phosphoethanolamine-N-(7-nitro-2-1,3-benzoxadiazol-4-yl) (PE-NBD), N-[1-(2,3-dioleoyloxy)propyl]-N,N,N-trimethylammonium methyl-sulfate (DOTAP) were purchased from Avanti Polar Lipids, propidium iodide, 5(6)-carboxyfluorescein, dynasore, wortmannin, nocodazole, pitstop2, genistein, methyl-β-cyclodextrin (MβCD), sodium azide (NaN_3), doxorubicin hydrochloride (DOX), cholesterol was purchased from Sigma-Aldrich. DMEM growth medium, and fetal bovine serum were purchased from Sigma- Aldrich. L-glutamine, penicillin, and streptomycin were purchased from Thermo Fisher Scientific. Sephadex G25 size-exclusion PD-10 Columns were purchased from GE-Healthcare.

Lipopeptide, peptide dimers synthesis, and purification

All peptides were synthesized using Fmoc chemistry on a CEM Liberty Blue microwave-assisted peptide synthesizer. The synthesis of peptides E4-GW, K4-GW, and lipopeptides CPE4, and CPK4 was described in Chapter 2.

For the synthesis of Fluo-K4 and Fluo-E4, two additional glycine residues were coupled to the N-terminus of the peptides on resin, before fluorescein was manually coupled by the addition of 0.2 mmol 5(6)-carboxyfluorescein, 0.4 mmol HCTU and 0.6 mmol DIPEA in 3 mL DMF. The reaction was shaken at room temperature overnight, the peptide was cleaved from the resin using 3 mL of a cleavage mixture (TFA:triisopropylsilane:H_2O=95:2.5:2.5%) and shaken for 1.5 hours. The peptides were precipitated by pouring the reaction mixture into 45 mL cold diethyl ether (-20 ℃) and isolated by centrifugation. The crude peptides were redissolved in H_2O (20 mL) and lyophilized.

K4-dimer synthesis routes are shown in **SI Scheme 1**, and all the peptide sequences are listed in **Table S1**. A Tentagel HL RAM resin (0.22 mmol/g) was used for peptide synthesis. The Fmoc group was removed with 20% piperidine in DMF by heating to 90 ℃ for 1 min. In the reaction, 5 eqv. of DIC and 5 eqv. Oxyma and 5 eqv. of amino acid were added to the reaction vessel and heated to 90 ℃ and kept for 4 minutes. DMF was used as the solvent. Except for the lipidated and fluorescent peptides, all peptides were acetylated at the N-terminus.

Synthesis of PK4: K4GW-Cys14 (66 mg, 20 μmol) was dissolved in water (15 mL) and added dropwise to 2,2′-Dithiobis(5-nitropyridine) (62 mg, 200 μmol) dissolved in 5 mL of acetone and stirred overnight. The yellow reaction mixture was filtered and dried under a N_2 flow. The crude peptide was dissolved in water (20 mL) and purified by HPLC (see below), after lyophilization K4GW-Cys14-S-nitropyridine was obtained as a solid powder (50 mg, 14.5 μmol, yield: 72.5%). K4GW-Cys14-S-nitropyridine (20 mg, 5.8 μmol) was mixed with peptide K4-Cys14 (20 mg, 6.6 μmol) in 10 mL HEPES buffer (pH 8.1). The solution turned yellow gradually and after 30 minutes the peptide was purified by injecting the reaction mixture into the HPLC (see below). After lyophilization, a white powder was obtained of PK4 (22mg, 3.5 μmol, yield: 59.8%).

Synthesis of NK4: CG-K4GW (70 mg, 20 μmol) was dissolved in 15 mL of water in a flask and 5 mL 2,2′-Dithiobis(5-nitropyridine) (62mg, 200 μmol) solution in acetone was added dropwise while stirring. After filtration, the reaction mixture was dried under N_2 flow. The crude peptide was dissolved in 20 mL water and purified by HPLC (see below) and lyophilized yielding a white CG-K4GW-S-nitropyridine solid powder (60 mg, 16.5 μmol, yield: 82%). Peptide CG-K4GW-S-nitropyridine (20 mg, 5.5 μmol) was mixed with peptide CG-K4 (20 mg, 6.2 μmol) and dissolved in 10 mL HEPES buffer (pH 8.1). The solution turned yellow gradually and after 30 minutes, the peptide was purified by directly injecting the reaction mixture into the HPLC (see below) and lyophilization to yield a white powder (20 mg, 3 μmol, yield: 54.2%).

Synthesis of CK4: WG-K4GC (70 mg, 20 μmol) was dissolved in 15 mL of water in a flask and 5 mL 2,2′-Dithiobis(5-nitropyridine) (62 mg, 200 μmol) solution in acetone was added dropwise while stirring. After filtration, the reaction mixture was dried under N_2 flow. The crude peptide was dissolved in 20 mL water and purified by HPLC (see below) and lyophilized yielding a white WG-K4GC-S-nitropyridine solid powder (55 mg, 15,7 μmol, yield: 78%). Peptide WG-K4GC-S-nitropyridine (20 mg, 5.5 μmol) was mixed with peptide K4-GC (20 mg, 6.2 μmol) and dissolved in 10 mL HEPES buffer (pH 8.1). The solution turned yellow gradually and after 30 minutes, the peptide was purified by directly injecting the reaction mixture into the HPLC (see below) and lyophilized to yield a white powder (18 mg, 2.7 μmol, yield: 48.8%).

Peptides were purified by HPLC on a Shimadzu system consisting of two KC-20AR pumps and an SPD-20A or SPD-M20A detector equipped with a Kinetix Evo C18 column. Eluents consisted of 0.1% TFA in water (A) and 0.1% TFA in MeCN (B), with all peptides eluted using a gradient of 20-90% B over 35 minutes, with a flow rate of 12 mL/min. Collected fractions were checked for purity via LC-MS, with the pure fractions being pooled and lyophilized. LC-MS spectra were recorded using a Thermo Scientific TSQ quantum access MAX mass detector connected to an Ultimate 3000 liquid chromatography system fitted with a 50x4.6 mm Phenomenex Gemini 3 μm C18 column. All peptides were characterized by LC-MS, see **Table S2**.

Circular dichroism comparison of coiled-coil peptide dimers interaction

CD spectra were recorded on a JASCO J-815 CD spectrometer fitted with a Peltier temperature controller. Ac-K4GW, and Ac-E4GW were dissolved in H_2O and diluted in PBS to a concentration of 10 μM separately, the same procedure was used for Ac-PK4GW, Ac-NK4GW, Ac-CK4GW groups with a concentration of 5 μM. The CD spectrum was baseline corrected with PBS. Unless otherwise specified, samples were measured at 20℃ in a quartz cuvette with a 2 mm path length. Spectra were recorded from 200 to 250 nm at 1 nm intervals, with a bandwidth of 1 nm, with the final spectrum consisting of the average of 5 sequentially recorded spectra. The mean residue molar ellipticity (θ, $deg \cdot cm^2 \cdot dmol^{-1}$) was calculated according to equation ($[\theta] = (100 * [\theta]obs)/(c * n * l)$), [θ]obs representing the observed ellipticity in mdeg, c is the peptide concentration in mM, n is the number of peptide bonds and l is the path length of the cuvette in cm. The percentage of helicity of the peptides (F_{helix}) can be calculated by equation: F_{helix} =100% ($[\theta]_{222}$ - $[\theta]_0$) / ($[\theta]_{max}$ - $[\theta]_0$), $[\theta]_{222}$ represents the mean residue molar ellipticity of peptide at 222 nm, $[\theta]_0$ is the mean residue ellipticity of the peptide when the peptide is in an entirely random coil conformation, $[\theta]_{max}$ is the maximum theoretical mean residue ellipticity (**Table S3**).

Fluorescent peptide labeling experiments

Cell culture: HeLa, and CHO cells purchased from ATCC were cultured according to ATCC guidelines. The DMEM growth medium containing sodium bicarbonate, without sodium pyruvate and HEPES, was supplemented with 10% fetal bovine serum, 1% of L-glutamine, and 1% penicillin/streptomycin, at 37 °C in the presence of 5% CO_2.

HeLa cells were seeded on 8-well confocal plates at the density of $5*10^4$ cells/well on the day before experiments were performed. After 18 h incubation, CPK4 and CPE4 lipopeptides (10 μM, 200 μL) were added to the cells and incubated for 1-2 h. After the removal of the medium and washing 3 times with PBS, the medium containing PK4, NK4, and CK4 dimers were added and incubated for 15 min, then washed 3 times, fluorescein-E4 peptide (10 μM, 200 μL) was added and incubated for 15 min, washed 3 times and supplemented with phenol-red-free medium before confocal imaging (Leica TCS SP8). Quantification of interaction differences was conducted by flow cytometry (Guava easyCyte) with cells seeded on 24-well plates at $2.5*10^5$ cells/well, then the same procedure was followed before measuring.

Liposome preparation and characterization

NBD-PE labeled liposomes: lipids were dissolved in $CHCl_3$ in the molar ratio DOPC, DOPE, and cholesterol 2:1:1 (total lipid concentration, 1 mM, with 1 mol% of NBD-PE) was dissolved in $CHCl_3$. The solvent was evaporated, and then lipids were hydrated with 1X PBS, and sonicated at 55°C for 3 min. CPE4-modified liposomes were made by adding 1 mol% of CPE4 into the lipid film.

PI encapsulated liposomes: lipids were dissolved in $CHCl_3$ in the molar ratio DOPC, DOPE, and cholesterol of 2:1:1 (total lipid concentration, 1 mM, 1 mol% of NBD-PE). Then lipids were hydrated with propidium iodide (10 mg/mL dissolved in PBS, 1 mL), then sonicated at 55°C for 3 min. Free PI was removed by size exclusion chromatography using a Sephadex G25 size-exclusion PD-10 Columns.

DOX encapsulated liposomes: lipids were dissolved in $CHCl_3$ in the molar ratio DOPC, DOPE, cholesterol 2:1:1 [total lipid concentration] = 4 mM. Liposomes were prepared by mixing the appropriate amount of lipids in a glass vial and evaporating the solvents under air to form lipid films. These films were hydrated with 20 mM citrate buffer (pH 2.5) and extruded 11 times with 200 nm pores. The citrate buffer was replaced by PBS (pH 7.4) through Sephadex G25 size-exclusion PD-10 Columns. Doxorubicin (DOX) was added to the liposomes at a drug-to-lipid molar ratio of 1:3 and subsequently rotated overnight. Free DOX was removed by size exclusion chromatography using a Sephadex G25 size-exclusion PD-10 Columns. The DOX concentration was determined using UV−vis spectrophotometry with a standard curve of different DOX concentrations. The liposomes were post-modified with CPE4. For this, lipopeptides in 1X PBS were added to the DOX-loaded liposomes [final CPE4] = 1 mol%, vortexed for 1 minute, and incubated for another 2 h at RT before use.

All liposomes were characterized by dynamic light scattering (DLS) at 25 °C to determine the average diameter (see **Table S4**).

Cellular uptake efficiency experiments

Flow cytometry analysis of cellular uptake efficiency was carried out using peptide-modified

liposomes to compare the uptake efficiency differences. CPK4 and CPE4 lipid films were made, hydrated with complete DMEM, and sonicated for 10 min at room temperature (final concentration is 10 μM). For cellular uptake efficiency study, HeLa cells were seeded on 24-well plates at the density of $2.5*10^5$ cells/well 18 h in advance, then pretreated with a medium containing CPK4 or CPE4 for 1-2 h (10 μM, 500 μL), after the removal of medium, PK4, NK4, CK4 dimers (5 μM, 500 μL) were added and incubated for 15 min, and the cells were washed 3 times with PBS, NBD labeled liposomes modified with CPE4 (CPE4-Liposome-NBD) were added to the cells (200 μM, 500 μL) and after 15 min incubation, the medium was removed and cells were washed with PBS 3 times, then digested with trypsin, washed, and resuspended in 1X PBS, followed by flow cytometry measurements.

Propidium iodide (PI) cellular delivery

HeLa cells were seeded on 8-well confocal plates at a density of $5*10^4$ cells/well. After 18 h, the cells were preincubated with a micellar solution of CPK4 and CPE4 (10 μM, 200 μL) for 1-2 h. After the removal of the medium and washing 3 times with PBS, the medium containing dimers PK4, NK4, and CK4 was added (5 μM, 200 μL) and incubated for 15 minutes, and the cells were washed 3 times with PBS before NBD-PE labeled CPE4-liposomes containing PI were added and incubated for 15 min. Next, the cells were washed 3 times with PBS, supplemented with the phenol-red-free medium, and cultured another 30 min before confocal imaging.

Doxorubicin uptake experiment

To test the delivery of liposomal doxorubicin (DOX) with different dimers, HeLa cells were seeded on 8-well confocal plates at a density of $5*10^4$ cells/well the day before the experiment. After 18 h, HeLa cells were preincubated with a medium containing CPK4, and CPE4 for 1-2 h (10 μM, 200 μL), and subsequently exposed to the medium containing PK4, NK4, or CK4 dimer (5 μM, 200 μL) and incubated for 15 min. After removal of the medium and 3 times washing with PBS, CPE4 decorated liposomes encapsulating DOX were added and incubated for another 15 min. Cells were washed 3 times and supplemented with phenol-red-free medium and cultured another 30 min before confocal imaging. Quantification of DOX uptake followed a similar procedure in which cells were seeded in 96-well plates at the density of $2*10^4$ cells/well, then followed the same treatment of peptides and CPE4-liposomes encapsulated DOX (CPE4-Liposome-DOX) before flow cytometry measurements.

DOX uptake efficiency after endocytosis inhibitors incubation

To test the cellular uptake pathway of liposomal doxorubicin (DOX) delivery of PK4, HeLa cells were seeded on a 96-well plate at the density of $2*10^4$ cells/well the day before the experiment. After 18 h, HeLa cells were preincubated with CPE4 (10 μM, 100 μL) for 2 h, and subsequently exposed to different endocytosis inhibitors: nocodazole (40 μM), wortmannin (0.25 μM), dynasore (80 μM), pitstop2 (20 μM), genistein (200 μM), methyl-β-cyclodextrin (MβCD, 10 mM) sodium azide (0.1% w/v) in DMEM medium (100 μL) together with fresh CPE4 for 2 h. The medium was removed and replaced by a medium containing PK4 dimer (5 μM, 100 μL) and incubated for 15 min. After the removal of the medium and 3 times washing with PBS, CPE4 decorated liposomes containing DOX were added and incubated for another 15 min (200 μM, 100 μL). Cells were washed 3 times and incubated for 30 min and analyzed by flow cytometry. The 4 ℃ treatment was carried out by putting the cells into the fridge and then following the same procedure as above. The uptake mechanism of cells without CPE4 pretreatment was carried out the same way by using CPE4 modified liposomes

without DOX encapsulation.

For comparison, NBD-labeled cationic DOTAP liposomes (DOTAP: DOPC, 1:1, 1 mol% PE-NBD) were used to study the cellular uptake efficiency in the presence of endocytosis inhibitors. Cells were pretreated with different endocytosis inhibitors for 2 h, after removal of the medium DOTAP liposomes (200 μM, 100 μL) were added and cultured for 2 h, then analyzed by flow cytometry.

Cell viability measurements

The cytotoxicity of the peptides and liposomes in the absence of DOX was determined by a MTT assay. HeLa cells were seeded on a 96-well plate at a density of $1.0*10^4$ cells/well, HeLa cells were incubated with a medium containing CPK4, CPE4 (10 μM, 100 μL) for 2 h. After the removal of the medium and 3 times washing with PBS, different dimers PK4, NK4, and CK4 (5 μM, 100 μL) were added to the cells and incubated for 15 min, then cells were washed 3 times (PBS), and treated with a series of diluted CPE4 decorated liposomes without DOX encapsulation for 2h, the concentration of liposomes ranged from 500 μM to 0. 01 μM (500 μM, 300 μM, 150 μM, 75 μM, 30 μM, 15 μM, 7.5 μM, 3 μM, 1.5 μM, 0.75 μM, 0.3 μM, 0.15 μM, 0.05 μM, 0.01 μM). Next, the medium was removed from the wells, and cells were incubated in a fresh medium for another 36 h. After that, the MTT reagent was added to cells (final concentration is 0.5 mg/mL) and incubated for 4 h. Next, 50 uL medium was removed and 100 uL of DMSO was added to solubilize the purple formazan crystals and the spectrophotometric absorbance of the samples was measured using a microplate reader (Tecan Infinite M1000). The absorbance at 570 nm was measured with a reference wavelength at 650 nm. HeLa cells without any treatment were set at 100% cell survival.

For the cell viability assay after DOX delivery, HeLa cells were seeded on a 96-well plate at a density of $1.0*10^4$ cells/well, then incubated with a medium containing CPK4, CPE4 (10 μM, 100 μL) for 2 h. After the removal of the medium and 3 times washing with PBS, different dimers PK4, NK4, and CK4 (5 μM, 100 μL) were added to the cells and incubated for 15 min. Then cells were treated with a series of diluted CPE4 decorated liposomes loaded with DOX; the final concentration of DOX in the liposomes ranged from 100 μM to 0.01 μM (100 μM, 50 μM, 25 μM, 10 μM, 5 μM, 2.5 μM, 1 μM, 0.5 μM, 0.25 μM, 0.1 μM, 0.05 μM, 0.01 μM). After 2 h, all the medium was removed from the wells, and cells were incubated in a fresh medium for 36 h before the MTT assay.

Statistical analysis

All experiments were performed at least in triplicate (n=3) unless specified otherwise, and the significance was determined using an unpaired student t-test or two-way ANOVA analysis (Graphpad Prism). (****$P < 0.0001$; ***$P < 0.001$; **$P < 0.01$; *$P < 0.05$)

References

1. Farokhzad, O. C.; Langer, R., Nanomedicine: Developing smarter therapeutic and diagnostic modalities. *Advanced Drug Delivery Reviews* **2006,** *58* (14), 1456-1459.

2. Jain, R. K.; Stylianopoulos, T., Delivering nanomedicine to solid tumors. *Nature Reviews Clinical Oncology* **2010,** *7* (11), 653-664.

3. Scheinberg, D. A.; Villa, C. H.; Escorcia, F. E.; McDevitt, M. R., Conscripts of the infinite armada:

systemic cancer therapy using nanomaterials. *Nature Reviews Clinical Oncology* **2010,** *7* (5), 266-276.
4. Shi, J.; Kantoff, P. W.; Wooster, R.; Farokhzad, O. C., Cancer nanomedicine: progress, challenges and opportunities. *Nature Reviews Cancer* **2017,** *17* (1), 20-37.
5. Zhang, C.; Yan, L.; Wang, X.; Zhu, S.; Chen, C.; Gu, Z.; Zhao, Y., Progress, challenges, and future of nanomedicine. *Nano Today* **2020,** *35*, 101008.
6. Wolfram, J.; Ferrari, M., Clinical Cancer Nanomedicine. *Nano Today* **2019,** *25*, 85-98.
7. Canton, I.; Battaglia, G., Endocytosis at the nanoscale. *Chemical Society Reviews* **2012,** *41* (7), 2718-2739.
8. Sahay, G.; Alakhova, D. Y.; Kabanov, A. V., Endocytosis of nanomedicines. *Journal of Controlled Release* **2010,** *145* (3), 182-195.
9. Ruoslahti, E., Tumor penetrating peptides for improved drug delivery. *Advanced Drug Delivery Reviews* **2017,** *110-111*, 3-12.
10. Zhang, C.; Wu, W.; Li, R.-Q.; Qiu, W.-X.; Zhuang, Z.-N.; Cheng, S.-X.; Zhang, X.-Z., Peptide-Based Multifunctional Nanomaterials for Tumor Imaging and Therapy. *Advanced Functional Materials* **2018,** *28* (50), 1804492.
11. Jang, S.; Hyun, S.; Kim, S.; Lee, S.; Lee, I.-S.; Baba, M.; Lee, Y.; Yu, J., Cell-Penetrating, Dimeric α-Helical Peptides: Nanomolar Inhibitors of HIV-1 Transcription. *Angewandte Chemie International Edition* **2014,** *53* (38), 10086-10089.
12. Copolovici, D. M.; Langel, K.; Eriste, E.; Langel, Ü., Cell-Penetrating Peptides: Design, Synthesis, and Applications. *ACS Nano* **2014,** *8* (3), 1972-1994.
13. Meade, B. R.; Dowdy, S. F., Exogenous siRNA delivery using peptide transduction domains/cell penetrating peptides. *Advanced Drug Delivery Reviews* **2007,** *59* (2), 134-140.
14. Cheng, H.; Zhu, J.-Y.; Xu, X.-D.; Qiu, W.-X.; Lei, Q.; Han, K.; Cheng, Y.-J.; Zhang, X.-Z., Activable Cell-Penetrating Peptide Conjugated Prodrug for Tumor Targeted Drug Delivery. *ACS Applied Materials & Interfaces* **2015,** *7* (29), 16061-16069.
15. Kauffman, W. B.; Fuselier, T.; He, J.; Wimley, W. C., Mechanism Matters: A Taxonomy of Cell Penetrating Peptides. *Trends in Biochemical Sciences* **2015,** *40* (12), 749-764.
16. Richard, J. P.; Melikov, K.; Vives, E.; Ramos, C.; Verbeure, B.; Gait, M. J.; Chernomordik, L. V.; Lebleu, B., Cell-penetrating peptides: a reevaluation of the mechanism of cellular uptake. *Journal of Biological Chemistry* **2003,** *278* (1), 585-590.
17. Schneider, A. F. L.; Kithil, M.; Cardoso, M. C.; Lehmann, M.; Hackenberger, C. P. R., Cellular uptake of large biomolecules enabled by cell-surface-reactive cell-penetrating peptide additives. *Nature Chemistry* **2021,** *13* (6), 530-539.
18. Nam, S. H.; Jang, J.; Cheon, D. H.; Chong, S.-E.; Ahn, J. H.; Hyun, S.; Yu, J.; Lee, Y., pH-Activatable cell penetrating peptide dimers for potent delivery of anticancer drug to triple-negative breast cancer. *Journal of Controlled Release* **2021,** *330*, 898-906.
19. Guo, X.; Wang, L.; Duval, K.; Fan, J.; Zhou, S.; Chen, Z., Dimeric Drug Polymeric Micelles with Acid-Active Tumor Targeting and FRET-Traceable Drug Release. *Advanced Materials* **2018,** *30* (3), 1705436.
20. Pescina, S.; Ostacolo, C.; Gomez-Monterrey, I. M.; Sala, M.; Bertamino, A.; Sonvico, F.; Padula, C.; Santi, P.; Bianchera, A.; Nicoli, S., Cell penetrating peptides in ocular drug delivery: State of the art. *Journal of Controlled Release* **2018,** *284*, 84-102.
21. Guidotti, G.; Brambilla, L.; Rossi, D., Cell-Penetrating Peptides: From Basic Research to Clinics. *Trends in Pharmacological Sciences* **2017,** *38* (4), 406-424.
22. Vale, N.; Duarte, D.; Silva, S.; Correia, A. S.; Costa, B.; Gouveia, M. J.; Ferreira, A., Cell-penetrating peptides in oncologic pharmacotherapy: A review. *Pharmacological Research* **2020,** *162*, 105231.
23. Desale, K.; Kuche, K.; Jain, S., Cell-penetrating peptides (CPPs): an overview of applications for improving

the potential of nanotherapeutics. *Biomaterials Science* **2021,** *9* (4), 1153-1188.
24. Zhang, F.; Angelova, A.; Garamus, V. M.; Angelov, B.; Tu, S.; Kong, L.; Zhang, X.; Li, N.; Zou, A., Mitochondrial Voltage-Dependent Anion Channel 1–Hexokinase-II Complex-Targeted Strategy for Melanoma Inhibition Using Designed Multiblock Peptide Amphiphiles. *ACS Applied Materials & Interfaces* **2021,** *13* (30), 35281-35293.
25. Kang, Z.; Ding, G.; Meng, Z.; Meng, Q., The rational design of cell-penetrating peptides for application in delivery systems. *Peptides* **2019,** *121*, 170149.
26. Südhof Thomas, C.; Rothman James, E., Membrane Fusion: Grappling with SNARE and SM Proteins. *Science* **2009,** *323* (5913), 474-477.
27. Jahn, R.; Scheller, R. H., SNAREs — engines for membrane fusion. *Nature Reviews Molecular Cell Biology* **2006,** *7* (9), 631-643.
28. Chen, Y. A.; Scheller, R. H., SNARE-mediated membrane fusion. *Nature Reviews Molecular Cell Biology* **2001,** *2* (2), 98-106.
29. Kong, L.; Askes, S. H. C.; Bonnet, S.; Kros, A.; Campbell, F., Temporal Control of Membrane Fusion through Photolabile PEGylation of Liposome Membranes. *Angewandte Chemie International Edition* **2016,** *55* (4), 1396-1400.
30. Yang, J.; Shimada, Y.; Olsthoorn, R. C. L.; Snaar-Jagalska, B. E.; Spaink, H. P.; Kros, A., Application of Coiled Coil Peptides in Liposomal Anticancer Drug Delivery Using a Zebrafish Xenograft Model. *ACS Nano* **2016,** *10* (8), 7428-7435.
31. Yang, J.; Bahreman, A.; Daudey, G.; Bussmann, J.; Olsthoorn, R. C. L.; Kros, A., Drug Delivery via Cell Membrane Fusion Using Lipopeptide Modified Liposomes. *ACS Central Science* **2016,** *2* (9), 621-630.
32. Daudey, G. A.; Shen, M.; Singhal, A.; van der Est, P.; Sevink, G. J. A.; Boyle, A. L.; Kros, A., Liposome fusion with orthogonal coiled coil peptides as fusogens: the efficacy of roleplaying peptides. *Chemical Science* **2021,** *12* (41), 13782-13792.
33. Rabe, M.; Aisenbrey, C.; Pluhackova, K.; de Wert, V.; Boyle, Aimee L.; Bruggeman, Didjay F.; Kirsch, Sonja A.; Böckmann, Rainer A.; Kros, A.; Raap, J.; Bechinger, B., A Coiled-Coil Peptide Shaping Lipid Bilayers upon Fusion. *Biophysical Journal* **2016,** *111* (10), 2162-2175.
34. Rabe, M.; Zope, H. R.; Kros, A., Interplay between Lipid Interaction and Homo-coiling of Membrane-Tethered Coiled-Coil Peptides. *Langmuir* **2015,** *31* (36), 9953-9964.
35. Rabe, M.; Schwieger, C.; Zope, H. R.; Versluis, F.; Kros, A., Membrane Interactions of Fusogenic Coiled-Coil Peptides: Implications for Lipopeptide Mediated Vesicle Fusion. *Langmuir* **2014,** *30* (26), 7724-7735.
36. Chatterjee, K.; Zhang, J.; Honbo, N.; Karliner, J. S., Doxorubicin Cardiomyopathy. *Cardiology* **2010,** *115* (2), 155-162.
37. Takemura, G.; Fujiwara, H., Doxorubicin-Induced Cardiomyopathy: From the Cardiotoxic Mechanisms to Management. *Progress in Cardiovascular Diseases* **2007,** *49* (5), 330-352.
38. Vercauteren, D.; Piest, M.; van der Aa, L. J.; Al Soraj, M.; Jones, A. T.; Engbersen, J. F. J.; De Smedt, S. C.; Braeckmans, K., Flotillin-dependent endocytosis and a phagocytosis-like mechanism for cellular internalization of disulfide-based poly(amido amine)/DNA polyplexes. *Biomaterials* **2011,** *32* (11), 3072-3084.
39. Tao, W.; Mao, X.; Davide, J. P.; Ng, B.; Cai, M.; Burke, P. A.; Sachs, A. B.; Sepp-Lorenzino, L., Mechanistically Probing Lipid-siRNA Nanoparticle-associated Toxicities Identifies Jak Inhibitors Effective in Mitigating Multifaceted Toxic Responses. *Molecular Therapy* **2011,** *19* (3), 567-575.
40. Arcaro, A.; Wymann, M. P., Wortmannin is a potent phosphatidylinositol 3-kinase inhibitor: the role of phosphatidylinositol 3,4,5-trisphosphate in neutrophil responses. *Biochemical Journal* **1993,** *296* (2), 297-301.
41. Macia, E.; Ehrlich, M.; Massol, R.; Boucrot, E.; Brunner, C.; Kirchhausen, T., Dynasore, a Cell-Permeable Inhibitor of Dynamin. *Developmental Cell* **2006,** *10* (6), 839-850.

42. Doherty, G. J.; McMahon, H. T., Mechanisms of Endocytosis. *Annual Review of Biochemistry* **2009,** *78* (1), 857-902.
43. Preta, G.; Cronin, J. G.; Sheldon, I. M., Dynasore - not just a dynamin inhibitor. *Cell Communication and Signaling* **2015,** *13* (1), 24.
44. Delvendahl, I.; Vyleta, Nicholas P.; von Gersdorff, H.; Hallermann, S., Fast, Temperature-Sensitive and Clathrin-Independent Endocytosis at Central Synapses. *Neuron* **2016,** *90* (3), 492-498.
45. von Kleist, L.; Stahlschmidt, W.; Bulut, H.; Gromova, K.; Puchkov, D.; Robertson, Mark J.; MacGregor, Kylie A.; Tomilin, N.; Pechstein, A.; Chau, N.; Chircop, M.; Sakoff, J.; von Kries, Jens P.; Saenger, W.; Kräusslich, H.-G.; Shupliakov, O.; Robinson, Phillip J.; McCluskey, A.; Haucke, V., Role of the Clathrin Terminal Domain in Regulating Coated Pit Dynamics Revealed by Small Molecule Inhibition. *Cell* **2011,** *146* (3), 471-484.
46. Rejman, J.; Bragonzi, A.; Conese, M., Role of clathrin- and caveolae-mediated endocytosis in gene transfer mediated by lipo- and polyplexes. *Molecular Therapy* **2005,** *12* (3), 468-474.
47. Vercauteren, D.; Vandenbroucke, R. E.; Jones, A. T.; Rejman, J.; Demeester, J.; De Smedt, S. C.; Sanders, N. N.; Braeckmans, K., The Use of Inhibitors to Study Endocytic Pathways of Gene Carriers: Optimization and Pitfalls. *Molecular Therapy* **2010,** *18* (3), 561-569.
48. Rodal, S. K.; Skretting, G.; Garred, Ø.; Vilhardt, F.; van Deurs, B.; Sandvig, K., Extraction of Cholesterol with Methyl-β-Cyclodextrin Perturbs Formation of Clathrin-coated Endocytic Vesicles. *Molecular Biology of the Cell* **1999,** *10* (4), 961-974.
49. Novakowski, S.; Jiang, K.; Prakash, G.; Kastrup, C., Delivery of mRNA to platelets using lipid nanoparticles. *Scientific Reports* **2019,** *9* (1), 552.
50. Yao, C.; Wang, P.; Li, X.; Hu, X.; Hou, J.; Wang, L.; Zhang, F., Near-Infrared-Triggered Azobenzene-Liposome/Upconversion Nanoparticle Hybrid Vesicles for Remotely Controlled Drug Delivery to Overcome Cancer Multidrug Resistance. *Advanced Materials* **2016,** *28* (42), 9341-9348.
51. Marsh, M.; Helenius, A., Virus Entry: Open Sesame. *Cell* **2006,** *124* (4), 729-740.

Supporting Information

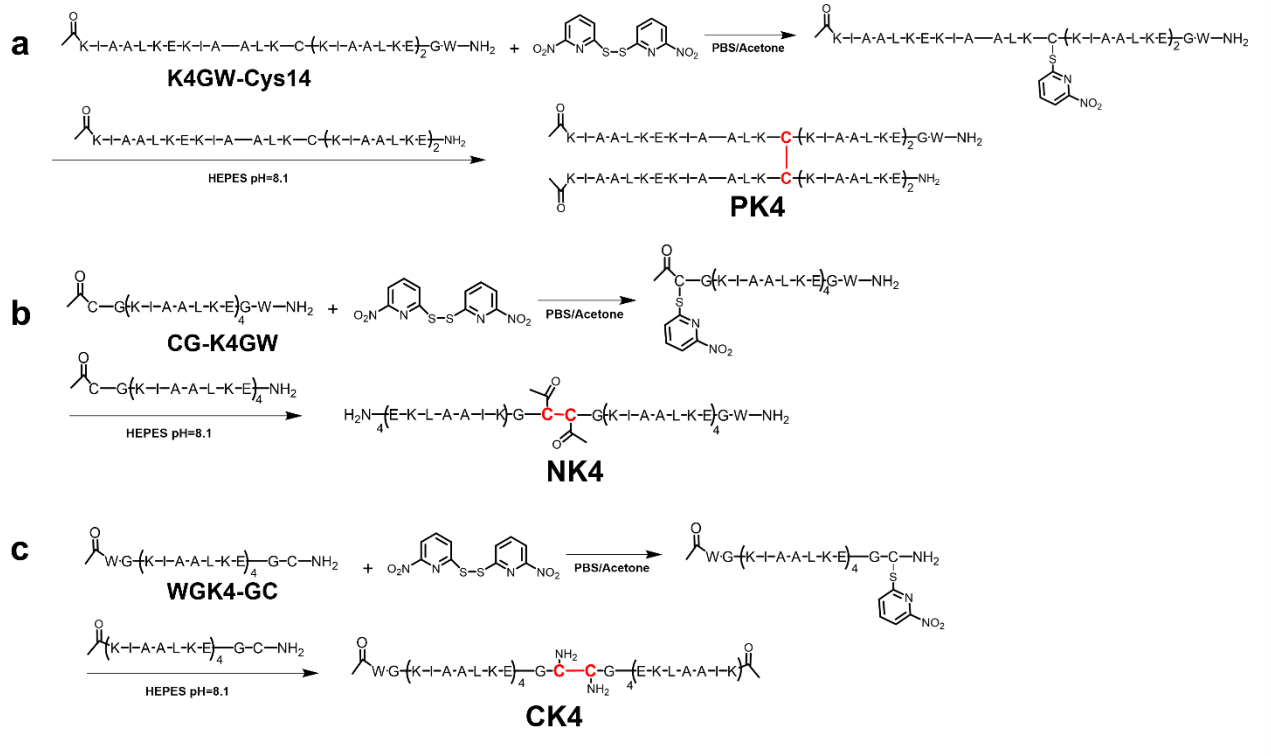

SI scheme 1. (a) Synthetic route of K4-dimers, **(a)** PK4, **(b)** NK4, and **(c)** CK4.

Table S1. Sequences of peptides used in this work

Peptides	Sequences					
	ef	*gabcdef*	*gabcdef*	*gabcdef*	*gabcdef*	*ga*
K4		KIAALKE	KIAALKE	KIAALKE	KIAALKE	GW-NH_2
E4		EIAALEK	EIAALEK	EIAALEK	EIAALEK	GW-NH_2
Fluo-K4	Fluo-GG	KIAALKE	KIAALKE	KIAALKE	KIAALKE	GW-NH_2
Fluo-E4	Fluo-GG	EIAALEK	EIAALEK	EIAALEK	EIAALEK	GW-NH_2
K4-Cys14		KIAALKE	KIAALKC	KIAALKE	KIAALKE	-NH_2
K4GW-Cys14		KIAALKE	KIAALKC	KIAALKE	KIAALKE	GW-NH_2
CG-K4	CG	KIAALKE	KIAALKE	KIAALKE	KIAALKE	-NH_2
CG-K4GW	CG	KIAALKE	KIAALKE	KIAALKE	KIAALKE	GW-NH_2
K4-GC		KIAALKE	KIAALKE	KIAALKE	KIAALKE	GC-NH_2
WG-K4GC	WG	KIAALKE	KIAALKE	KIAALKE	KIAALKE	GC-NH_2

Table S2. Theoretical and observed mass of peptides using LC-MS

Peptide	Mass(calculated)/Da	Mass(Found)/Da
PK4	$[M+5H]^{5+}$ 1268.2	1267.5
	$[M+4H]^{4+}$ 1585.0	1584.3
	$[M+3H]^{3+}$ 2113.0	2113.0
	$[M+5H]^{5+}$ 1342.4	1341.8
NK4	$[M+4H]^{4+}$ 1677.8	1677.2
	$[M+3H]^{3+}$ 2236.7	2237.5
	$[M+5H]^{5+}$ 1342.4	1341.8
CK4	$[M+4H]^{4+}$ 1677.8	1677.9
	$[M+3H]^{3+}$ 2236.7	2237.5
Fluo-E4	$[M+3H]^{3+}$ 1252.7	1250.6
	$[M+2H]^{2+}$ 1878.5	1876.0
Fluo-K4	$[M+3H]^{3+}$ 1251.2	1249.3
	$[M+2H]^{2+}$ 1876.5	1874.0
CPK4	$[M+3H]^{3+}$ 1246.2	1244.3
	$[M+2H]^{2+}$ 1869.4	1866.4
CPE4	$[M+3H]^{3+}$ 1247.8	1245.4
	$[M+2H]^{2+}$ 1871.2	1868.8

Table S3. Normalized mean residue molar ellipticity and percentage helicity of peptides

Peptide	[θ] / deg cm^2 dmol^{-1}	Helicity (%)[a]
K4	-29894.2	89
E4	-25063.8	80
PK4	-8550.3	25
NK4	-34322.4	92
CK4	-39613.2	105
PK4+E4	-34330.3	90
NK4+E4	-31438.4	83
CK4+E4	-35300.8	92

[a] The percentage of α-helicity was calculated using the equation in section of experimental **3**. The percentage of helicity of the peptides (F_{helix}) can be calculated by equation: F_{helix} =100% ($[\theta]_{222}$ - $[\theta]_0$) / ($[\theta]_{max}$ - $[\theta]_0$), $[\theta]_{222}$ represents the mean residue molar ellipticity of peptide at 222 nm, $[\theta]_0$ is the mean residue ellipticity of the peptide when the peptide is in an entirely random coil conformation, $[\theta]_{max}$ is the maximum theoretical mean residue ellipticity.

Table S4. Characterization of liposomes used in this study

Liposomes	Size(nm)	PDI	Zeta-potential(mV)
Liposome-NBD	121.0±3.9	0.168±0.042	-3.23±2.31
CPE4-liposome-NBD	96.7±5.2	0.129±0.023	-4.23±2.56
Liposome-NBD-PI	151.1±7.2	0.150±0.035	-4.87±1.23
CPE4-liposome-NBD-PI	157.2±5.8	0.105±0.021	-5.23±2.06
Liposome-NBD-Dox	146.2±4.8	0.116±0.034	-5.35±3.27
CPE4-liposome-NBD-Dox	171.6±2.8	0.093±0.043	-3.67±2.23
DOTAP-liposome-NBD	154.2±3.2	0.126±0.027	54.23±3.73

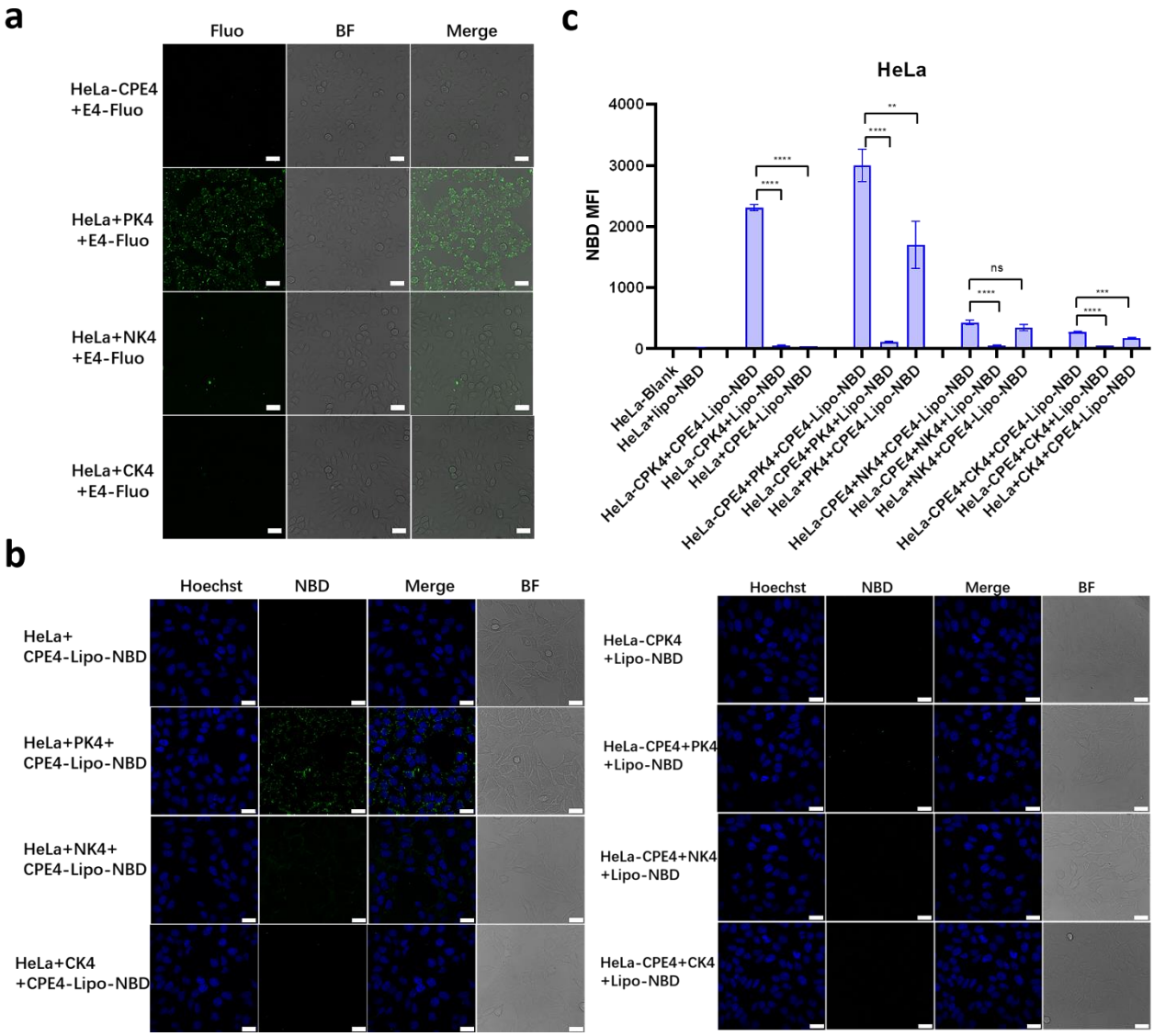

SI Figure 1. (a) Confocal images of cell membrane labeling between dimers and fluorescein-E4 of control groups. **(c)** Confocal images of K4 monomer and dimers with NBD-labeled liposomes modified with CPE4 of control groups. Green: NBD-PE; blue: Hoechst 33342; BF: bright field; scale bar is 30 μm. **(b)** Quantification of NBD-liposome intensity by flow cytometry of all groups. Unpaired student t-test was used to determine the significance of data comparisons (****P < 0.0001; ***P < 0.001; **P < 0.01; *P < 0.05). In all panels, error bars represent mean ± s.d. (n=3).

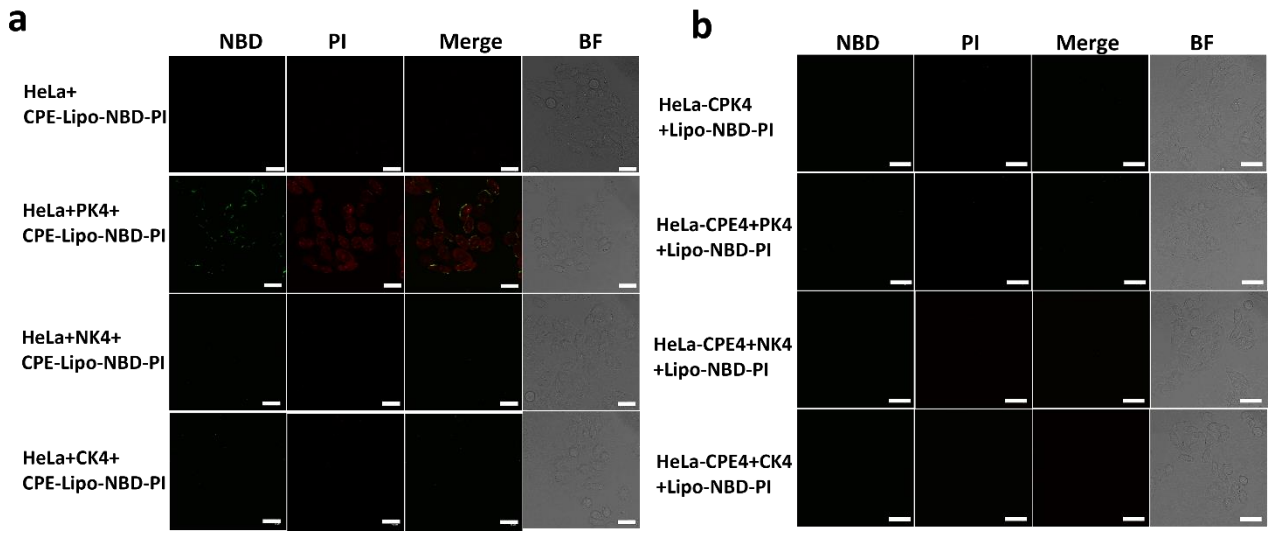

SI Figure 2. Confocal images of liposomal PI delivery by K4 monomer and dimers of control groups **(a)** cells without CPE4/CPK4 pretreatment **(b)** liposomes without CPE4 modification. Green: NBD-PE; red: PI; BF: bright field; scale bar is 30 μm.

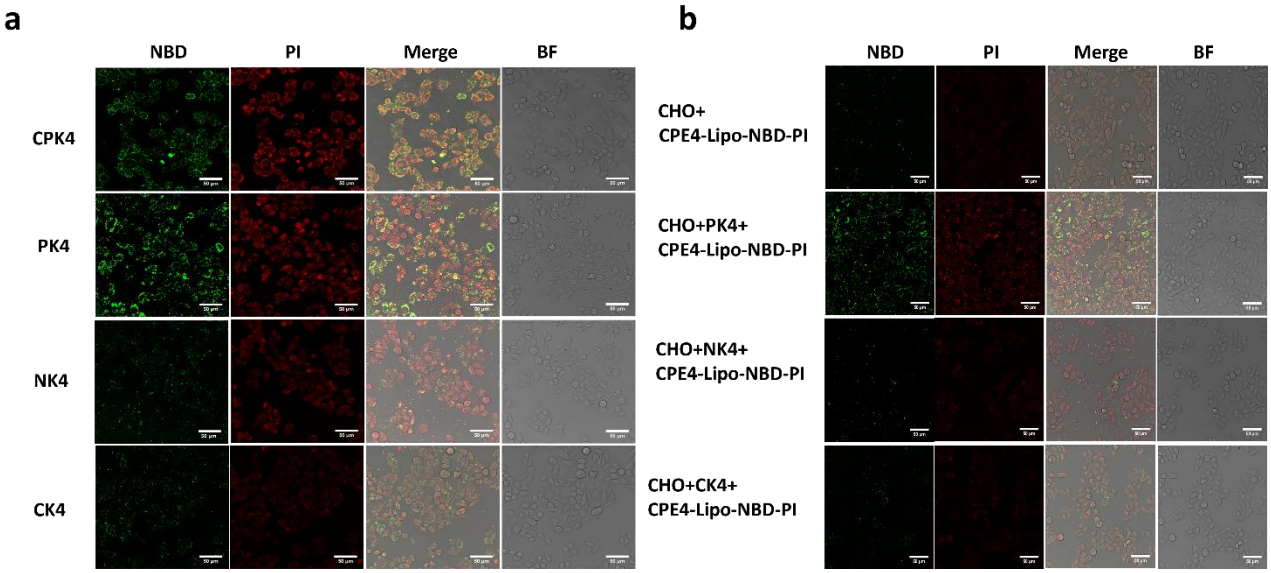

SI Figure 3. Confocal images of liposomal PI delivery by K4 monomer and dimers with the CHO cell line **(a)** cells with CPE4/CPK4 pretreatment **(b)** cells without CPE4/CPK4 pretreatment. Liposomes contain 1% NBD-PE and 1% CPE4 on the membrane and were loaded with 10 mg/mL PI. Green: NBD-PE; red: PI; BF: bright field; scale bar is 50 μm. CPK4: CPK4-cell+CPE4-liposome-NBD-PI; PK4: CPE4-cell+PK4+CPE4-liposome-NBD-PI; NK4: CPE4-cell+NK4+CPE4-liposome-NBD-PI; CK4: CPE4-cell+CK4+CPE4-liposome-NBD-PI.

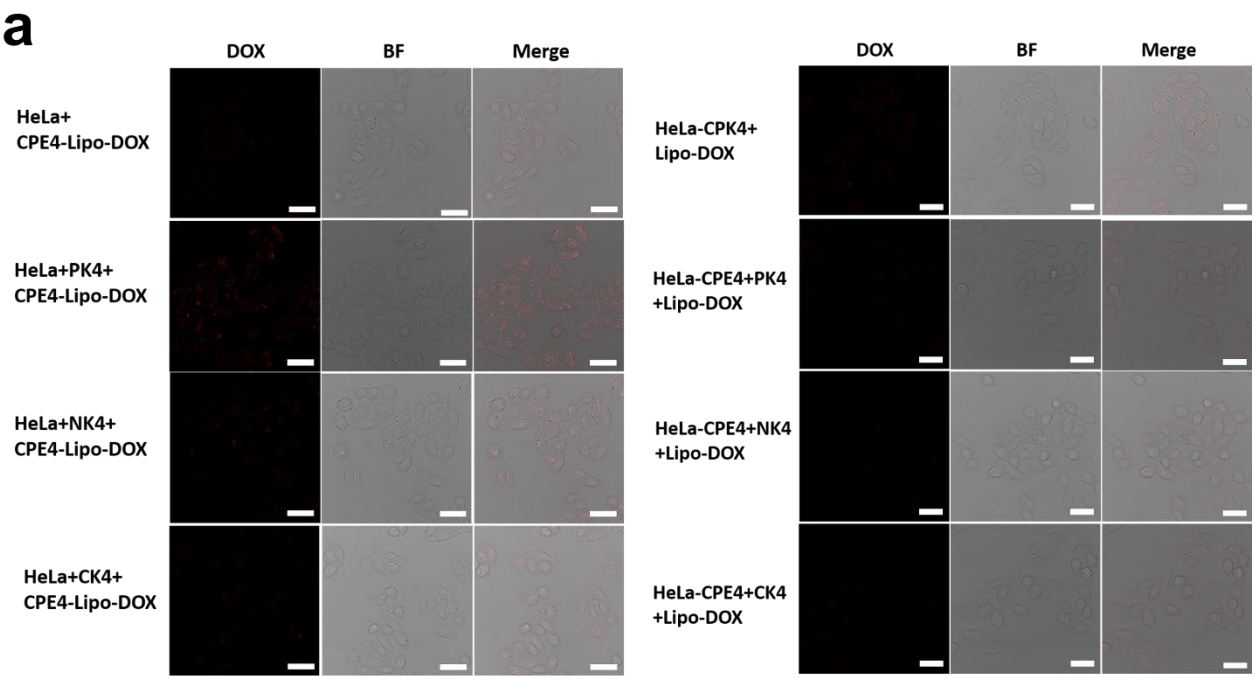
a
DOX
BF
Merge
HeLa+
CPE4-Lipo-DOX
HeLa+PK4+
CPE4-Lipo-DOX
HeLa+NK4+
CPE4-Lipo-DOX
HeLa+CK4+
CPE4-Lipo-DOX
HeLa-CPK4+
Lipo-DOX
HeLa-CPE4+PK4
+Lipo-DOX
HeLa-CPE4+NK4
+Lipo-DOX
HeLa-CPE4+CK4
+Lipo-DOX

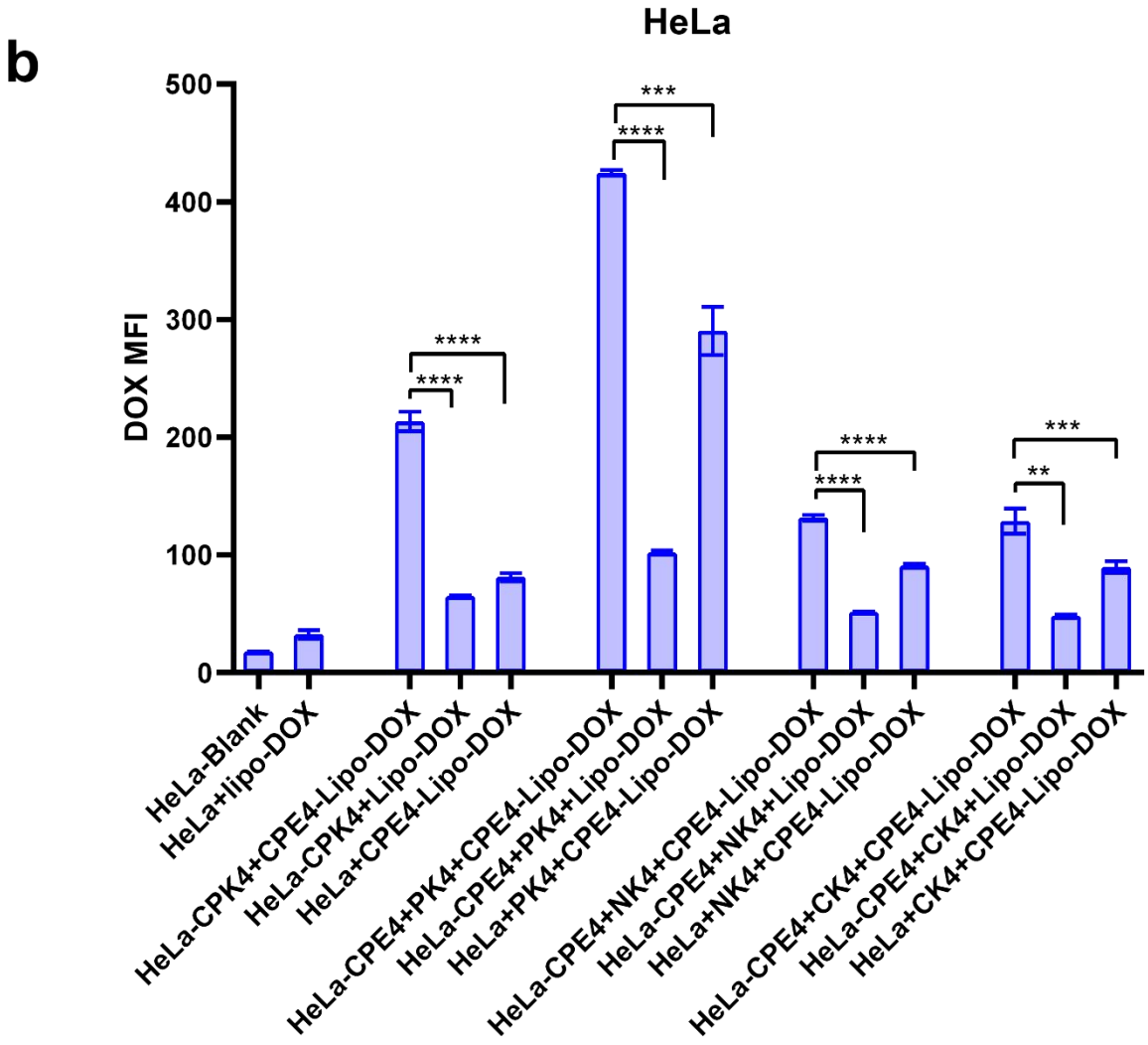
b
HeLa
DOX MFI
500
400
300
200
100
0
***
****
****
****
****
****
****
**
***
HeLa-Blank
HeLa+lipo-DOX
HeLa-CPK4+CPE4-Lipo-DOX
HeLa-CPK4+Lipo-DOX
HeLa+CPE4-Lipo-DOX
HeLa-CPE4+PK4+CPE4-Lipo-DOX
HeLa-CPE4+PK4+Lipo-DOX
HeLa+PK4+CPE4-Lipo-DOX
HeLa-CPE4+NK4+CPE4-Lipo-DOX
HeLa-CPE4+NK4+Lipo-DOX
HeLa+NK4+CPE4-Lipo-DOX
HeLa-CPE4+CK4+CPE4-Lipo-DOX
HeLa-CPE4+CK4+Lipo-DOX
HeLa+CK4+CPE4-Lipo-DOX

SI Figure 4. (a) Confocal images of DOX uptake of K4 monomer and dimers in HeLa cells of control groups. **(b)** Quantification of internalized DOX intensity of K4 monomer and dimers of all groups. Red: PI; BF: bright field; scale bar is 30 μm. Unpaired student t-test was used to determine the significance of data comparisons (****P < 0.0001; ***P < 0.001; **P < 0.01; *P < 0.05). In all panels, error bars represent mean ± s.d. (n=3).

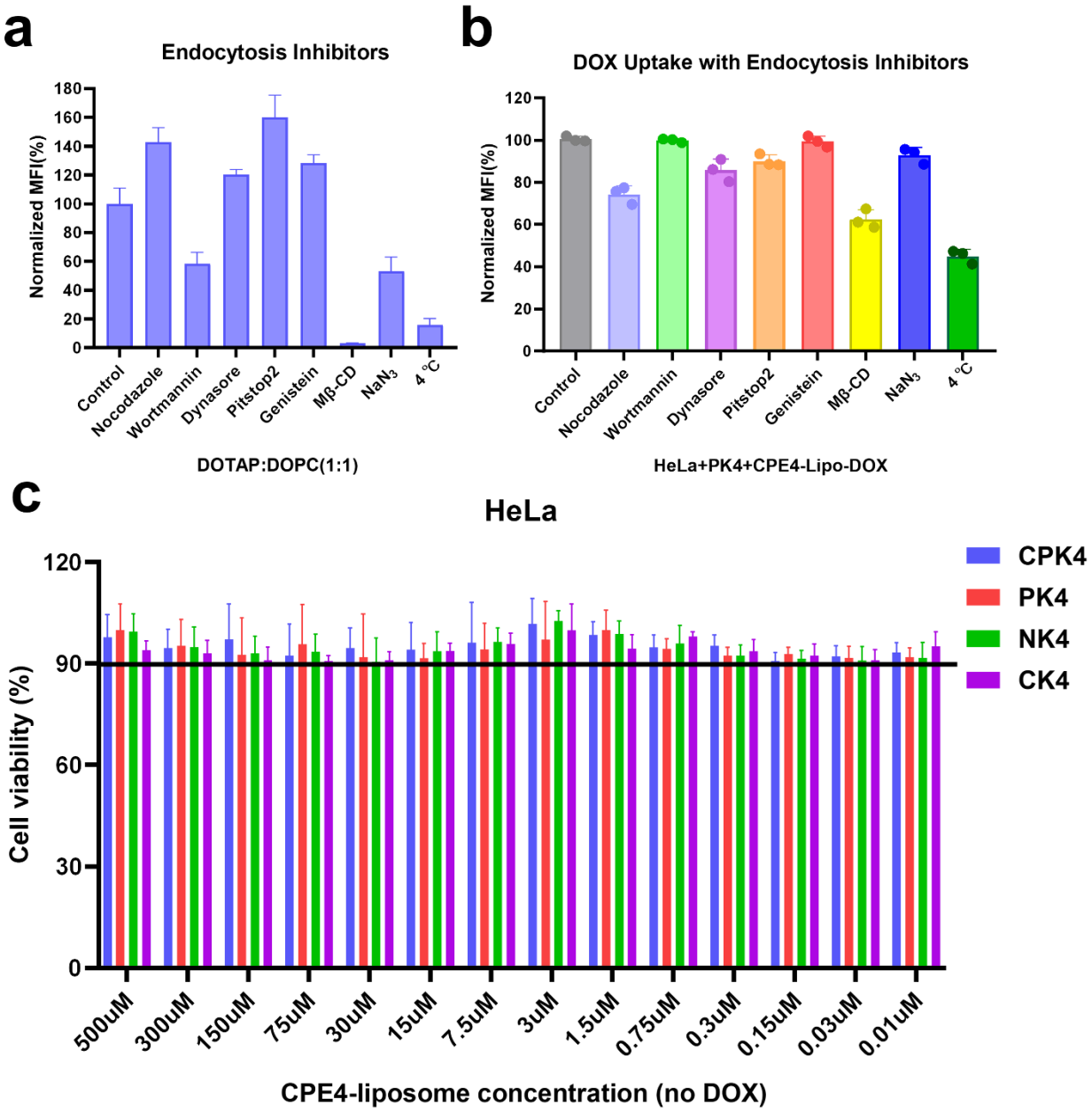

SI Figure 5. (a) Quantification of uptake efficiency of the cationic liposome DOTAP (DOTAP: DOPC=1:1, 1 mol% NBD-PE) with endocytosis inhibitors in HeLa cells. **(b)** Quantification of uptake efficiency of PK4 dimer with endocytosis inhibitors in HeLa calls without CPE4 pretreatment. **(c)** Cell viability of liposomes without DOX encapsulation. The solid line represents 90% cell viability. CPK4: CPK4-cell+CPE4-liposome; PK4: CPE4-cell+PK4+CPE4-liposome; NK4: CPE4-cell+NK4+CPE4-liposome; CK4: CPE4-cell+CK4+CPE4-liposome